International Journal of Research
Available at https://edupediapublications.org/journals
p-ISSN: 2348-6848
e-ISSN: 2348-795X
Volume 03 Issue 18
December2016

Statistical Analysis on Weld Bead Geometry of Pulsed Current Micro-plasma Arc Welded AISI 316Ti Austenitic Stainless Steel Sheets

[1]Ch. Swetha, [2]Dr. M. Murali Krishna
[1,2]Department of Mechanical Engineering, Sai Ganapathi Engineering College, Visakhapatnam, Andhra Pradesh, India

Abstract
Micro-plasma arc welding (MPAW) uses low amperage to join sheets, where the thickness is low, such that they can be used for manufacturing metal bellows, metal diaphragms etc. In the present work, pulsed current MPAW is used for joining 0.3 mm thick AISI 316Ti austenitic stainless steel sheets. Peak current, base current, pulse rate and pulse width are considered as input parameters and weld bead geometry parameters namely front width, back width, front height, back height are considered as output responses. Total 27 experiments are performed as per Box-Benhken design of response surface method. Weld bead geometry parameters are measured using metallurgical microscope. Empirical mathematical models are developed using statistical software (MINITAB). Analysis of variance (ANOVA) is carried out at 95% confidence level. Main and interaction effects are studied. Scatter plots are drawn to understand the variation of actual and predicted values of weld bead parameters.

Keywords: Pulsed current; micro-plasma arc welding; austenitic stainless steel; weld bead geometry; AISI 316Ti.

INTRODUCTION

In 1964 plasma arc welding process was introduced to the welding industry as a method of bringing better control to the arc welding process in lower current ranges [1]. It is used to produce high quality welds in both miniature and pre-precision applications and to provide long electrode life for high production requirements at all levels of amperage. Plasma welding is equally suited to manual and automatic applications. It is used in a variety of joining operations ranging from welding of miniature components to seam welding, to high volume production welding, and many others.

From the literature it is understood that Voropai *et al*. developed a technique of pulsed micro-plasma butt welding for welding shells of asbestos-metal gaskets made of aluminium of thickness 0.2–0.3 mm [2]. Pulsed micro-plasma welding results in steady burning of the arc on low current and in the destruction of the oxide film on the joined metal. In this method, argon of a purity of not less than 99.8% is used as plasma forming gas and helium of a purity of not less than 99.5% as protective gas. Sepokurov *et al.* developed a device for controlling welding current, so that it can be used for welding thin components and for hard facing small components [3]. Luo *et al.* analyzed the surface microstructure and

the anodic polarization curves in a 1 N H_2SO_4 solution of a 0Cr19Ni9 steel submerged arc welded joint before and after surface melting using a 4-A micro-plasma arc [4].

The results showed that both the heat-affected zone and the weld metal of the as-welded joint had a lower corrosion resistance than the as-received parent material, while the arc melted joint had a significantly increased corrosion resistance. This increase in corrosion resistance is attributed to a rapid solidification of the melted layer. Rapid solidification of the melted layer refines its microstructure, decreases micro-segregation and inhibits the precipitation of chromium carbides at the grain boundaries. Karimzadeh *et al*. investigated the effect of micro-plasma arc welding (MPAW) process parameters on grain growth and porosity distribution of thin sheet Ti6Al4V alloy weldment [5]. The MPAW procedure was performed at different current, welding speed and flow rates of shielding and plasma gas. Square-butt welding in a single pass, using direct current and straight polarity (DCEN) was selected for the welding process. The titanium alloy studied in the present experiment is a thin sheet of Ti6Al4V alloy with a thickness of 0.8 mm. Karimzadeh *et al.* examined the effect of epitaxial growth on microstructure of Ti-6Al-4V alloy weldment by artificial neural networks (ANNs) [6].

The micro-plasma arc welding (MPAW) procedure was performed at different currents, welding speeds and flow rates of shielding and plasma gas. Micro-structural characterizations were studied by optical and scanning electron microscopy (SEM). Finally, an artificial neural network was developed to predict grain size of fusion zone (FZ) at different currents and welding speeds. Xu *et al*. developed a model to simulate the electromagnetic phenomena and fluid field in plasma arc occurring during the low-current micro-plasma arc welding process [7]. They also discussed the effects of the nozzle neck-in and welding current of micro-plasma arc on the arc electromagnetic field distribution.

From the works reported on plasma arc welding, it is understood that most of the works reported were on higher thickness; very few works are reported on thickness less than0.3 mm. So, it is intended to study the effect of pulsed MPAW process parameters on weld bead geometry parameters of 0.3 mm thick austenitic stainless steel sheets of AISI 316 Ti, which are used for metal bellow manufacturing. Peak current, base current, pulse rate and pulse width are considered as input parameters and weld bead geometry parameters namely front width, back width, front height, back height are considered as output responses.

EXPERIMENTAL PROCEDURE

Weld specimens of 100x150x0.3 mm size are prepared from AISI 316Ti sheets and joined using square-butt joint. The chemical composition and tensile properties of AISI 316Ti stainless steel sheet, as provided by M/s Metallic Bellows (I) Pvt. Ltd., Chennai, India, are presented in Tables 1 and 2. Argon is used as a shielding gas and a trailing gas to avoid contamination from outside atmosphere. The welding conditions adopted during welding are presented in Table 3. From the earlier works carried out on pulsed current MPAW it was understood that the peak current, back current, pulse rate and pulse width are the dominating parameters which effect the weld

quality characteristics [8–11]. The values of process parameters used in this study are the optimal values obtained from our earlier papers [8–11]. Hence peak current, back current, pulse rate and pulse width are chosen as parameters and their levels are presented in Table 4. Details about experimental setup are shown in Figure 1.

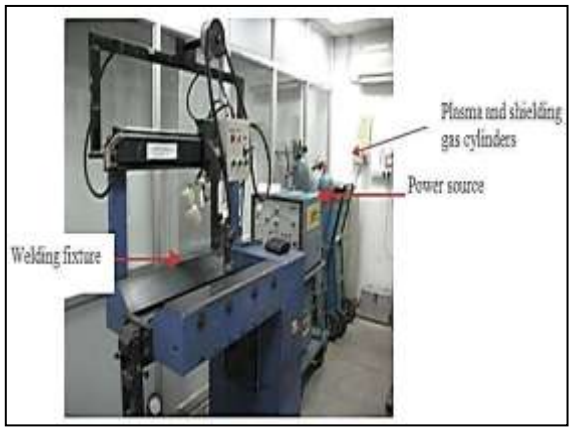

Fig. 1: *Micro-plasma Arc Welding Setup.*

MEASUREMENT OF WELD BEAD GEOMETRY

The weld pool geometries were measured using inverted trinocular metallurgical microscope, make: BS Pyromatic, model no.: BSPIL-MET-01013. Weld bead geometry for sample is presented in Figure 2.

Table 1: *Chemical Composition of AISI 316Ti (Weight %).*

C	Si	Mn	P	S	Cr	Ni	N	Ti
0.04	0.5	1.5	0.01	0.00	16.9	11.6	0.0	0.3

Table 2: *Mechanical Properties of AISI 316Ti.*

Elongation	**Yield Strength**	**Ultimate Tensile**
52.34	368.20	612.48

Table 3: *Welding Conditions.*

Power Source	**Secheron Micro-plasma Arc Machine (Model:**
Polarity	DCEN
Mode of operation	Pulse mode
Electrode	2% thoriated tungsten electrode
Electrode diameter	1 mm
Plasma gas	Argon and Hydrogen
Plasma gas flow rate	6 L/m
Shielding gas	Argon
Shielding gas flow rate	0.4 L/m
Purging gas	Argon
Purging gas flow rate	0.4 L/m
Copper nozzle diameter	1 mm

Nozzle to plate distance	1 mm
Welding speed	260 mm/min
Torch position	Vertical
Operation type	Automatic

Table 4: *Process Parameters and their Limits.*

		Leve		
Input Factor	**Units**	**–**	**0**	**+1**
Peak Current	Amp	6	7	8
Base Current	Amp	3	4	5
Pulse	Pulses/	2	4	60
Pulse	%	3	5	70

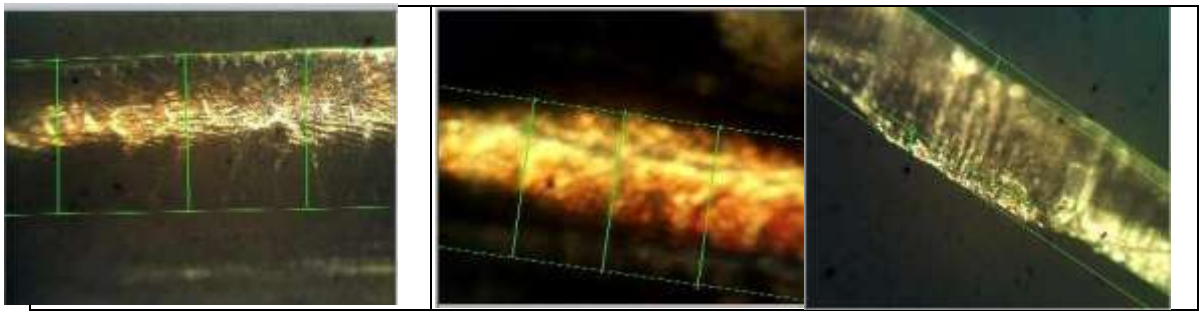

Front Width Back Width Front Height and Back Height

Fig. 2: *Weld Bead Geometry*

ANALYSIS OF EXPERIMENTAL DATA

The experiments were conducted as per the design matrix (Table 5) and the values of weld bead geometry measured by metallurgical microscopes are presented.

Front width=–617.874–
$169.830X_1+196.357X_2–17.232X_3+14.615X_4–$
$2.60X_1^2–48.439X_2^2+0.044X_3^2–$
$0.113X_4^2+19.876X_1X_2+2.734X_1X_3+0.537X_1X_4$
$+2.224X_2X_3+0.111X_2X_4–0.226X_3X_4$

Using MINITAB 14 statistical software package, the significant coefficients were determined and final model was developed using coefficients to estimate the front width, back width, front height and back height of weld joint

Front height=–
$843.460+243.770X_1 74.656X_2+1.037X_3–$
$0.292X_4–12.165X_1^2–5.410X_2^2–$
$0.009X_3^2+0.009X_4^2–11.792X_1X_2–0.533X_1X_3–$
$0.303X_1X_4+0.549X_2X_3–$
$0.369X_2X_4+0.017X_3X_4$

Back width=–481.946–
$132.469X_1+153.159X_2–13.441X_3+11.440X_4–$
$2.028X_1^2–38.094X_2^2+0.034X_3^2–$
$0.088X_4^2+15.503X_1X_2+2.132X_1X_3+0.149X_1X_4$
$+1.750X_2X_3+0.087X_2X_4–0.177X_3X_4$

International Journal of Research
Available at https://edupediapublications.org/journals
p-ISSN: 2348-6848
e-ISSN: 2348-795X
Volume 03 Issue 18
December2016

Back height=–
$522.954+151.137X_1+46.290X_2+0.643X_3-0.181X_4-7.540X_1^2-3.354X_2^2-0.006X_3^2+0.006X_4^2-7.311X_1X_2-0.330X_1X_3-0.188X_1X_4+0.341X_2X_3+0.229X_2X_4+0.010X_3X_4$
Where, X_1, X_2, X_3, X_4 are the coded values of peak current, base current, pulse rate and pulse width.

Table 5: *Experimental Results.*

Exp No.	Peak Current (Amp)	Base Current (Amp)	Pulse Rate (Pulses/sec)	Pulse Width (%)	Front Width (µm)	Back Width (µm)	Front Height (µm)	Back Height (µm)
1	6	3	40	50	479.096	373.695	122.391	75.882
2	8	3	40	50	446.984	348.648	103.269	64.027
3	6	5	40	50	614.698	479.464	118.42	73.420
4	8	5	40	50	662.089	516.429	52.131	32.321
5	7	4	20	30	506.935	395.409	102.469	63.531
6	7	4	60	30	706.965	551.433	62.043	38.467
7	7	4	20	70	607.208	473.622	137.931	85.517
8	7	4	60	70	444.836	346.972	134.511	83.397
9	6	4	20	50	455.249	355.094	115.863	71.835
10	8	4	60	50	796.629	621.371	82.417	51.099
11	6	4	20	50	586.09	457.150	106.875	66.263
12	8	4	20	50	464.808	362.550	111.625	69.208
13	7	3	60	30	595.7	464.646	108.486	67.261
14	7	5	40	30	547.117	426.751	101.271	62.788
15	7	3	40	50	524.36	409.001	99.82	61.888
16	7	5	40	50	459.257	358.220	88.332	54.766
17	6	4	40	30	562.102	438.440	115.354	71.519
18	8	4	40	30	486.24	379.267	126.638	78.516
19	6	4	40	70	494.861	385.992	134.511	83.397
20	8	4	40	70	461.973	360.339	121.587	75.384
21	7	3	20	50	479.096	373.695	163.231	101.203
22	7	5	20	50	446.984	348.648	115.776	71.781
23	7	3	60	50	514.698	401.464	114.815	71.185
24	7	5	60	50	662.089	516.429	121.486	75.321
25	7	4	40	50	586.09	457.150	138.183	85.673
26	7	4	40	50	564.808	440.550	132.124	81.917
27	7	4	40	50	595.7	464.646	130.248	80.754

Checking the Adequacy of the Developed Model

The adequacy of the developed model was tested using the analysis of variance technique (ANOVA) as shown in Table 6. As per this technique, if the calculated value of the F_{ratio} of the developed model is less than the standard F_{ratio} (from F-table) value at a desired level of confidence (say 95%), then the model is said to be adequate within the confidence limit.

Table 6: *Analysis of Variance.*

Analysis of Variance for Front Width (µm)						
Source	**DF**	**Seq SS**	**Adj SS**	**Adj MS**	**F**	**P**
Regression	14	140952	140952	10068	1.74	0.170
Linear	4	60010	13582	3396	0.59	0.678
Square	4	28396	14853	3713	0.64	0.642
Interaction	6	52546	52546	8758	1.52	0.254
Residual Error	12	69325	69325	5777		
Lack-of-Fit	9	60265	60265	6696	2.22	0.277
Pure Error	3	9060	9060	3020		
Total	26	210277				
Analysis of Variance for Back Width (µm)						
Source	**DF**	**Seq SS**	**Adj SS**	**Adj MS**	**F**	**P**
Regression	14	85755	85755	6125	1.74	0.170
Linear	4	36510	8264	2066	0.59	0.678
Square	4	17276	9037	2259	0.64	0.642
Interaction	6	31969	31969	5328	1.52	0.254
Residual Error	12	42177	42177	3515		
Lack-of-Fit	9	36666	36666	4074	2.22	0.277
Pure Error	3	5512	5512	1837		
Total	26	127932				
Analysis of Variance for Front Height (µm)						
Source	**DF**	**Seq SS**	**Adj SS**	**Adj MS**	**F**	**P**
Regression	14	8017.4	8017.37	572.67	1.10	0.438
Linear	4	4850.9	1473.02	368.25	0.71	0.602
Square	4	1363.5	1000.03	250.01	0.48	0.750
Interaction	6	1803.0	1803.03	300.50	0.58	0.742
Residual Error	12	6242.0	6242.05	520.17		
Lack-of-Fit	9	6167.3	6167.26	685.25	27.49	0.010
Pure Error	3	74.8	74.79	24.93		
Total	26	14259.4				
Analysis of Variance for Back Height (µm)						
Source	**DF**	**Seq SS**	**Adj SS**	**Adj MS**	**F**	**P**
Regression	14	3081.86	3081.86	220.133	1.10	0.438
Linear	4	1864.64	566.23	141.556	0.71	0.602
Square	4	524.12	384.42	96.104	0.48	0.750
Interaction	6	693.10	693.10	115.516	0.58	0.742
Residual Error	12	2399.41	2399.41	199.951		
Lack-of-Fit	9	2370.66	2370.66	263.407	27.49	0.010
Pure Error	3	28.74	28.74	9.581		
Total	26	5481.27				

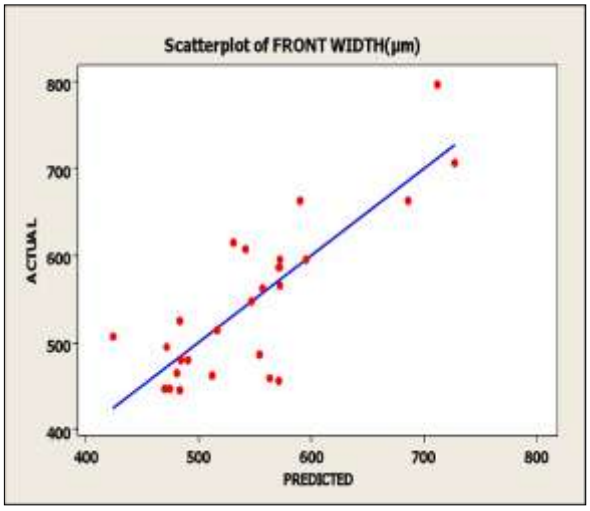

Fig. 3: *Scatter Plot for Front Width.*

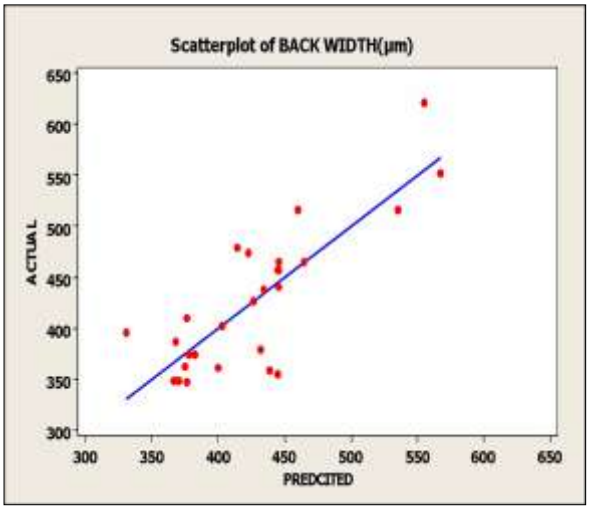

Fig. 4: *Scatter Plot for Back Width.*

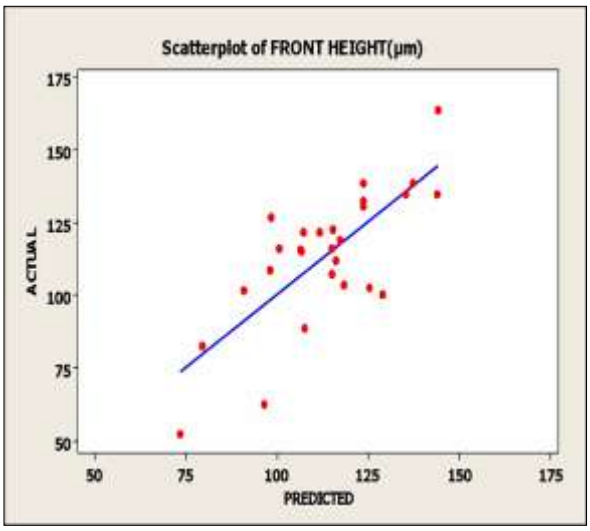

Fig. 5: *Scatter Plot for Front Width.*

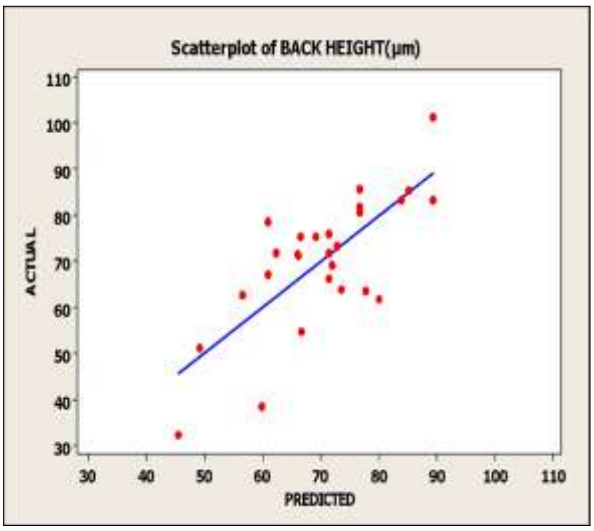

Fig. 6: *Scatter Plot for Back Height.*

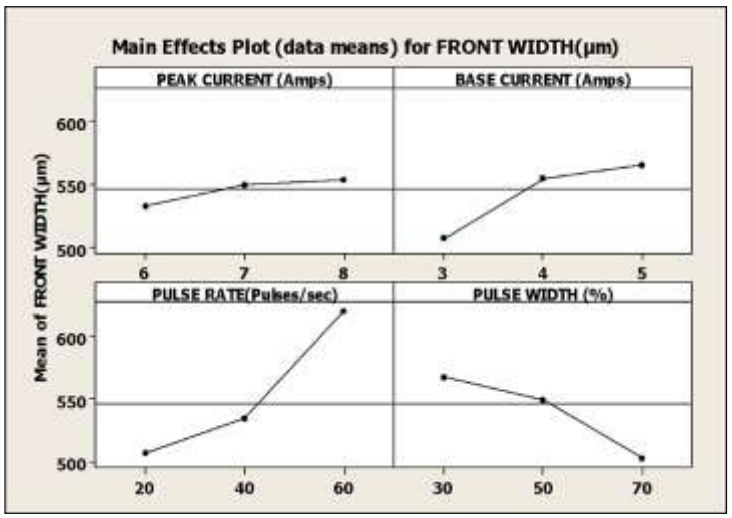

Fig. 7: *Main Effect on Front Width.*

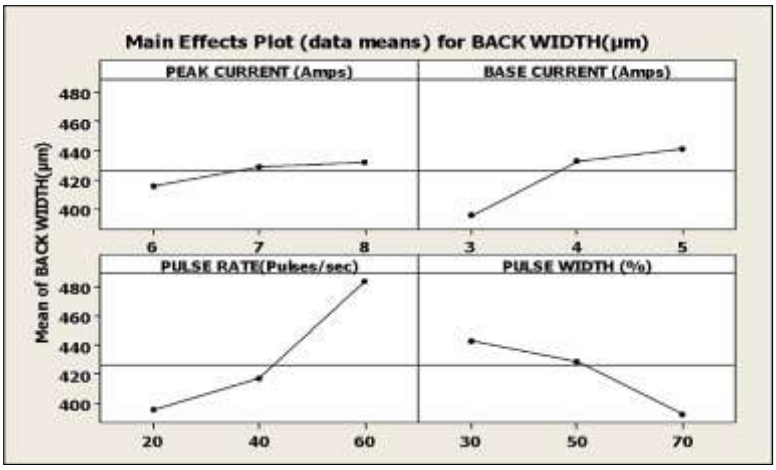

Fig. 8: *Main Effect on Back Width.*

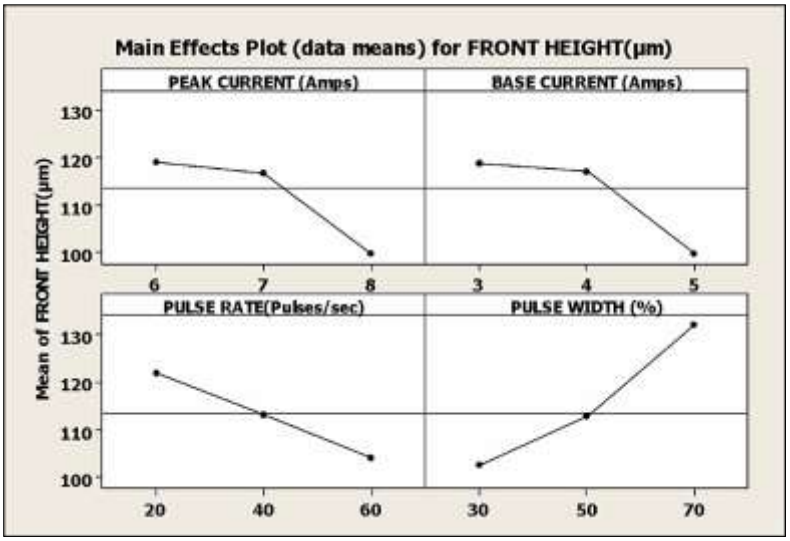

Fig. 9: *Main Effect on Front Height.*

Surface Plots

Surface plots are drawn to identify the optimal combination of input parameters, so that desired output response is achieved. Figures 11(a) to (f) represent the surface plots for front width.

From Figure 11(a), it is understood that front width is maximum at a peak current of 6 Amps and base current of 3 Amps.

From Figure 11(b), it is understood that front width is maximum at a peak current of 6 Amps and pulse rate of 60 pulses/sec.

From Figure 11(c), it is understood that front width is maximum at a peak current of 6 Amps and pulse width of 70%.

From Figure 11(d), it is understood that front width is maximum at a base current of 3 Amps and pulse rate of 20 pulses/sec.

From Figure 11(e), it is understood that front width is maximum at a base current of 3 Amps and pulse width of 70%.

From Figure 11(f), it is understood that front width is maximum at a pulse rate of 20 pulses/sec and pulse width of 70%.

From all the surface plots, it is understood that maximum front width can be achieved when peak current is 6 Amps, base current 3 Amps, pulse rate of 20 pulses/sec and pulse width of 70%.

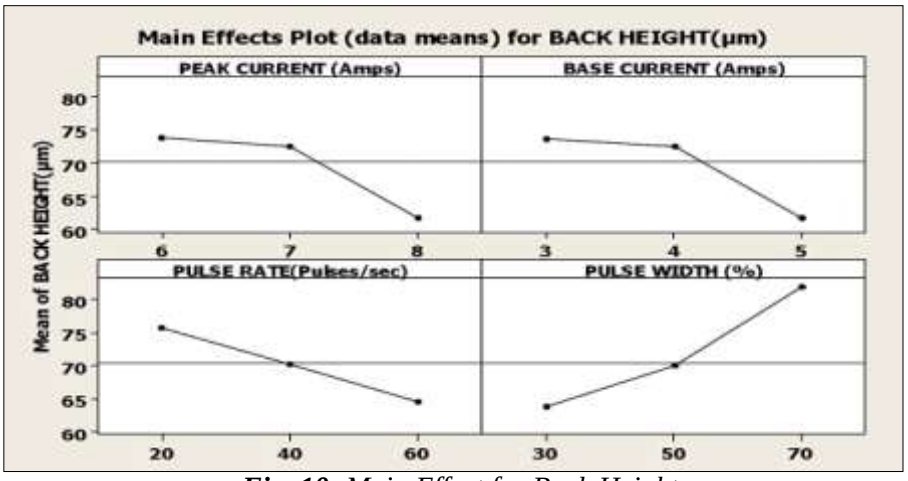

Fig. 10: *Main Effect for Back Height.*

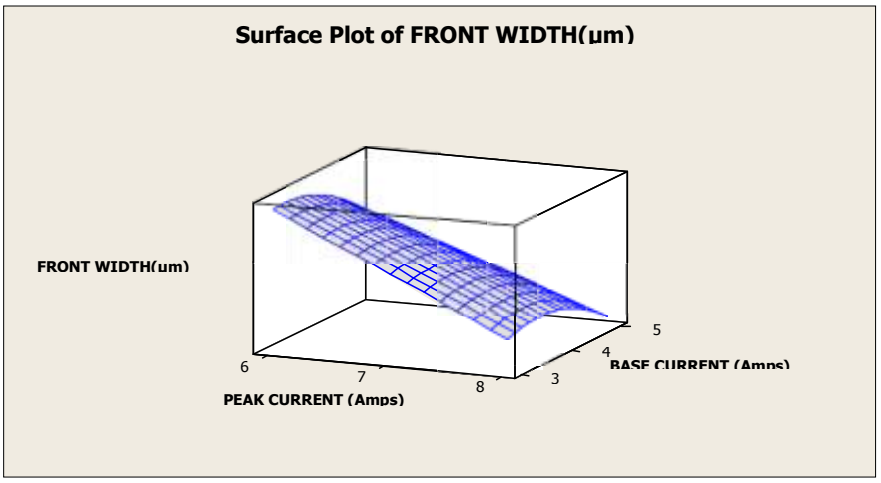

Fig. 11(a): *Surface plot for Front Width (Peak current versus Base Current).*

Fig. 11(b): *Surface plot for Front Width (Peak current versus Pulse Rate).*

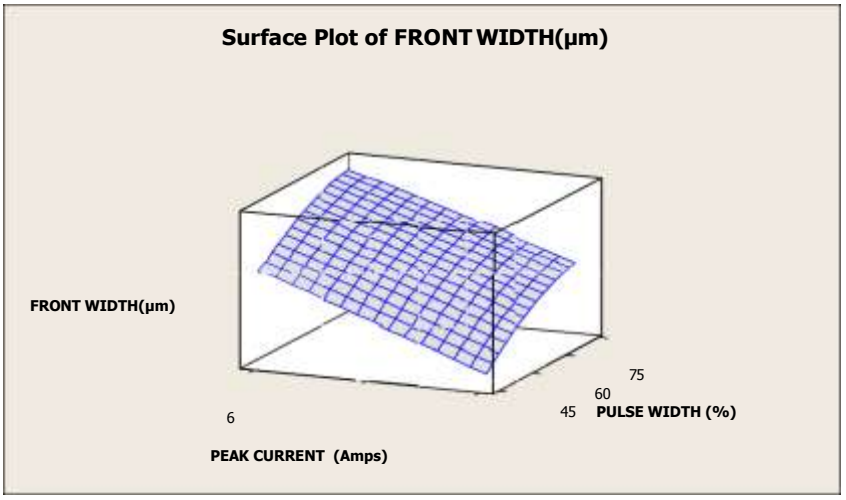

Fig. 11(c): *Surface plot for Front Width (Peak Current versus Pulse Width).*

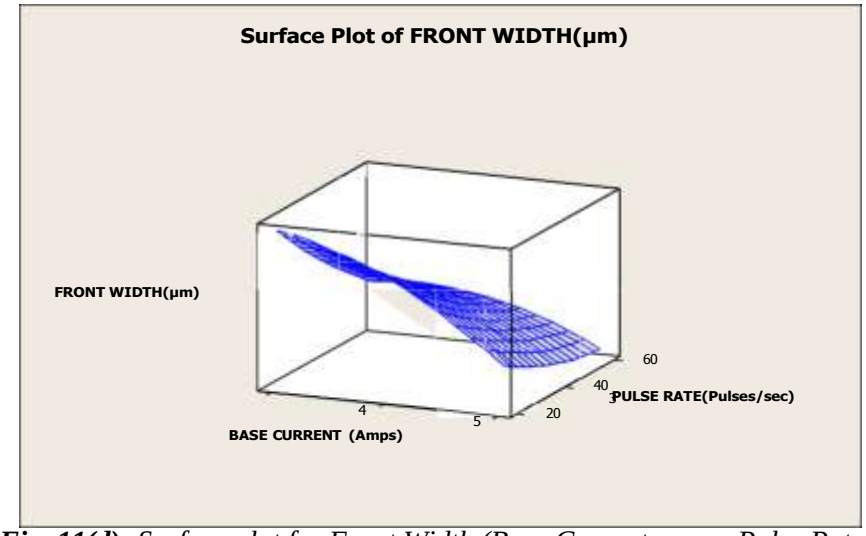

Fig. 11(d): *Surface plot for Front Width (Base Current versus Pulse Rate).*

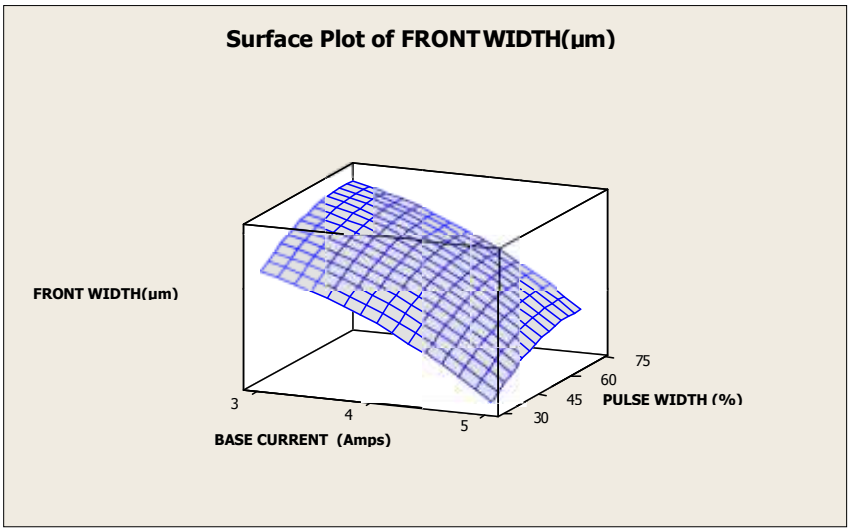

Fig. 11(e): *Surface plot for Front Width (Base Current versus Pulse Width).*

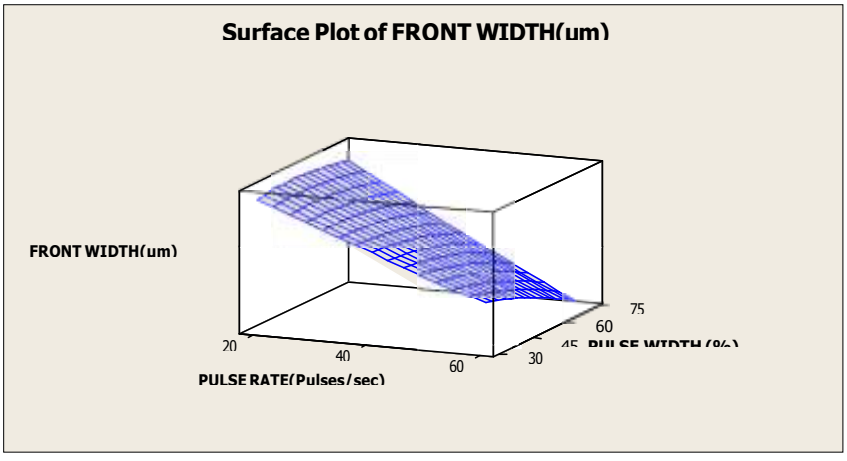

Figures 12(a) to (f) represent the surface plots for back width.

From Figure 12(a), it is understood that back width is maximum at a peak current of 6 Amps and base current of 3 Amps.

From Figure 12(b), it is understood that back width is maximum at a peak current of 6 Amps and pulse rate of 60 pulse/sec.

From Figure 12(c), it is understood that back width is maximum at a peak current of 6 Amps and pulse width of 70%.

From Figure 12(d), it is understood that back width is maximum at a base current of 3 Amps and pulse rate of 60 pulse/sec.

From Figure 12(e), it is understood that back width is maximum at a base current of 3 Amps and pulse width of 70%.

From Figure 12(f), it is understood that back width is maximum at a pulse rate of 20 pulses/sec and pulse width of 60%.

From all the surface plots, it is understood that back width is maximum when peak current is 6 Amps, base current is 3 Amps, pulse rate of 60 pulses/sec and pulse width of 70%.

Fig. 12(a): *Surface plot for Back Width (Peak current versus Base Current).*

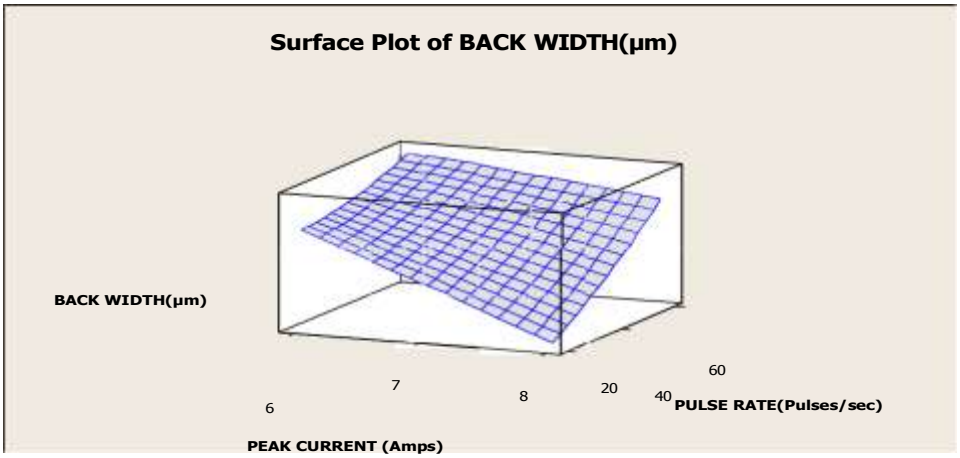

Fig. 12(b): *Surface plot for Back Width (Peak current versus Pulse Rate).*

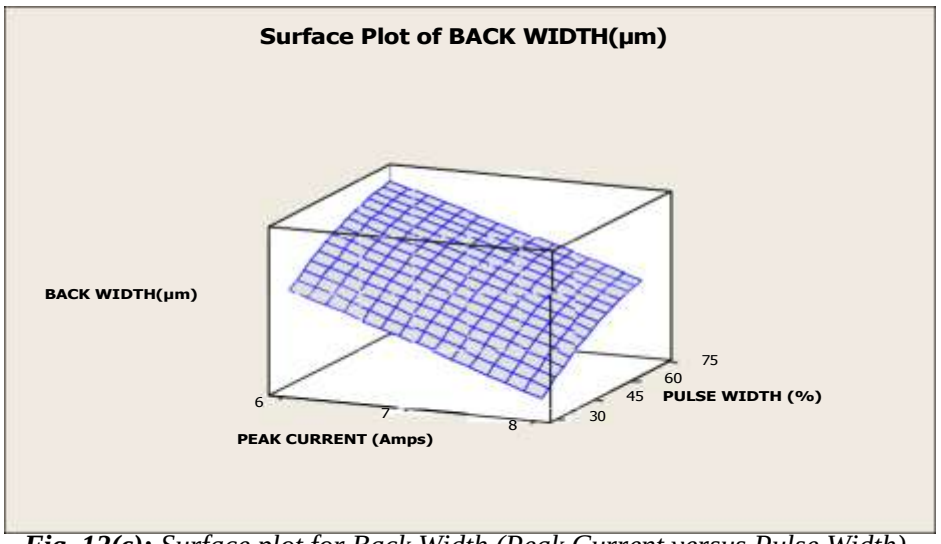

Fig. 12(c): *Surface plot for Back Width (Peak Current versus Pulse Width).*

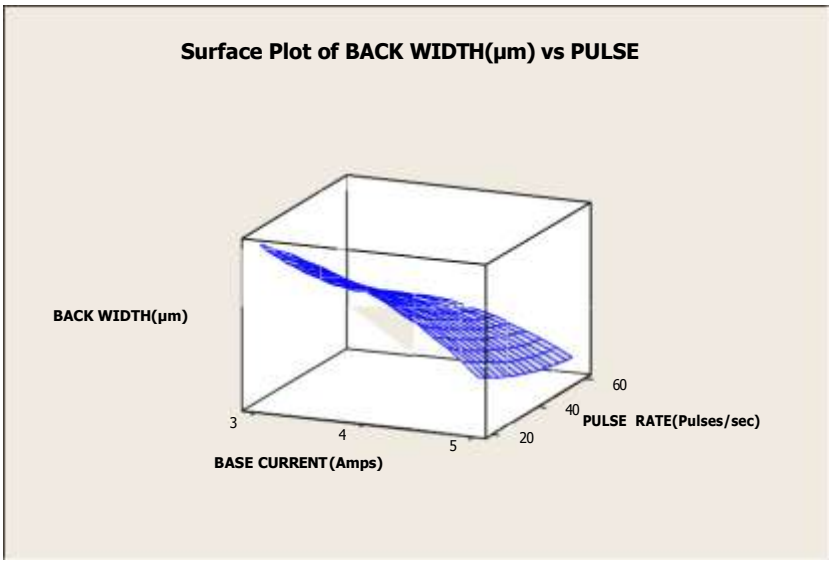

Fig. 12(d): *Surface plot for Back Width (Base Current versus Pulse Rate).*

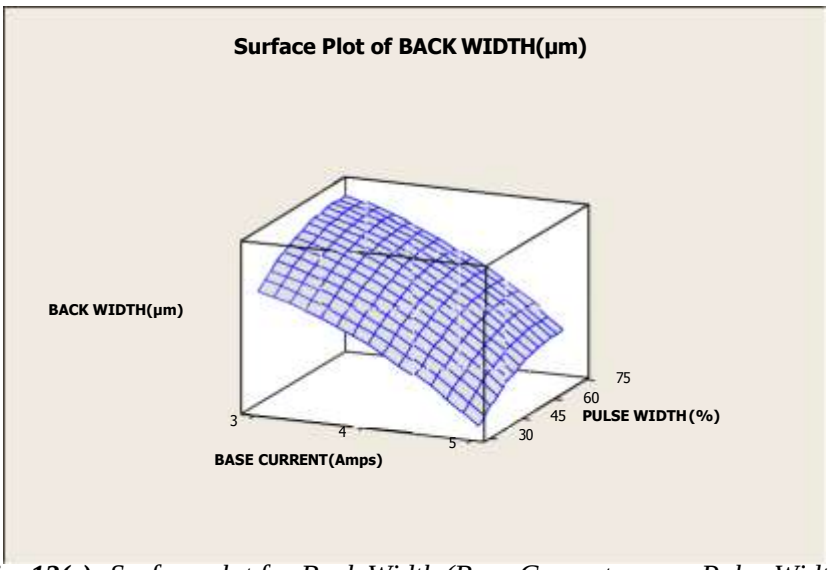

Fig. 12(e): *Surface plot for Back Width (Base Current versus Pulse Width).*

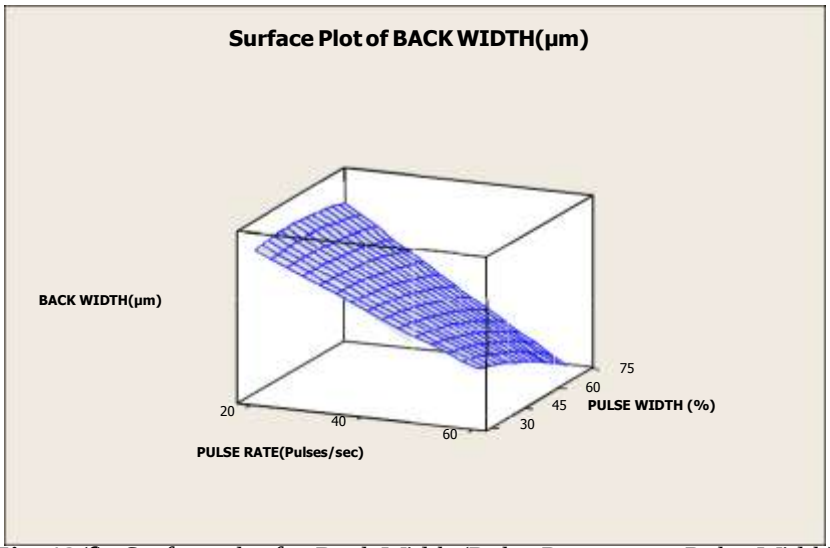

Fig. 12(f): *Surface plot for Back Width (Pulse Rate versus Pulse Width).*

Figures 13(a) to (f) represent the surface plots for front height.

From Figure 13(a), it is understood that front height is minimum at a peak current of 6 Amps and base current of 5 Amps.

From Figure 13(b), it is understood that front height is minimum at a peak current of 6 Amps and pulse rate of 60 pulses/sec.

From Figure 13(c), it is understood that front height is minimum at a peak current of 6 Amps and pulse width of 70%.

From Figure 13(d), it is understood that front height is maximum at a base current of 3 Amps and pulse rate of 60 pulses/sec.

From Figure 13(e), it is understood that front height is minimum at a base current of 3 Amps and pulse width of 60%.

From Figure 13(f), it is understood that front height is minimum at a pulse rate of 20 pulses/sec and pulse width of 60%.

From all the surface plots, it is understood that front height is minimum when peak current is 6 Amps, base current is 3 Amps, pulse rate of 60 pulses/sec and pulse width of 70%

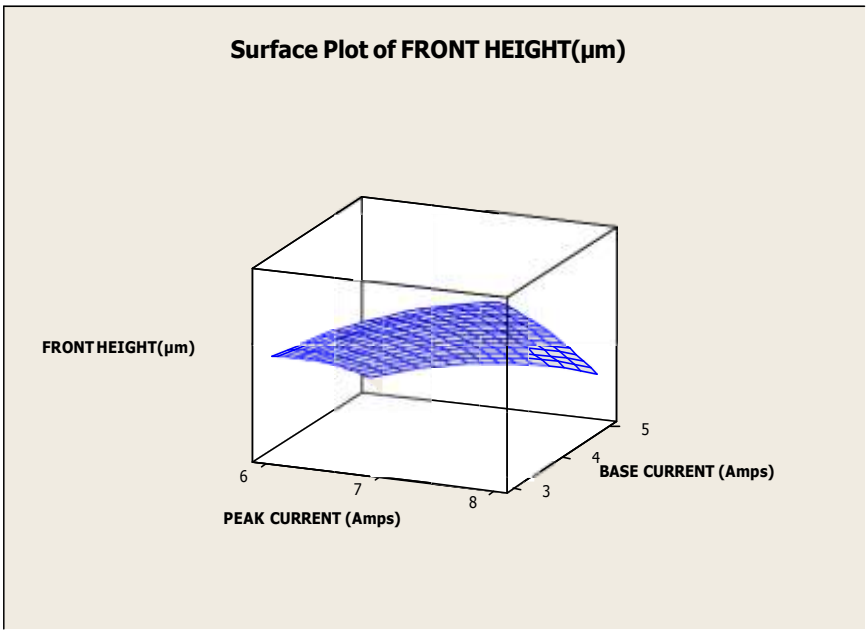

Fig. 13(a): *Surface plot for Front Height (Peak current versus Base Current).*

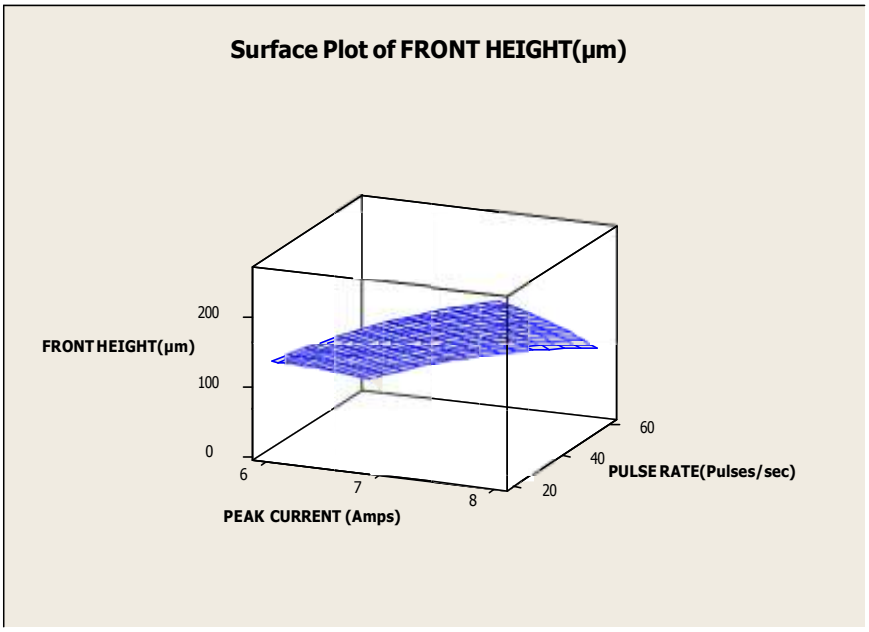

Fig. 13(b): *Surface plot for Front Height (Peak current versus Pulse Rate).*

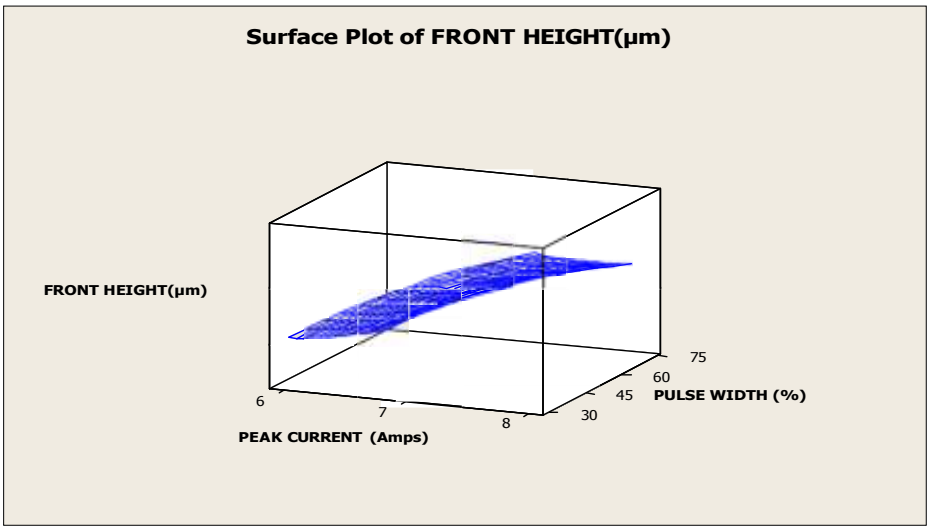

Fig. 13(c): *Surface plot for Front Height (Peak Current versus Pulse Width).*

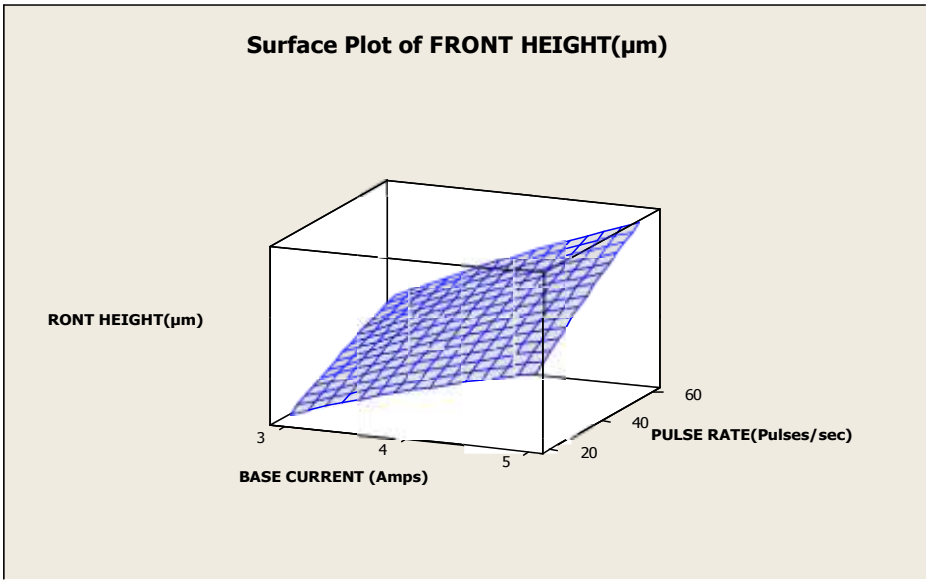

Fig. 13(d): *Surface plot for Front Height (Base Current versus Pulse Rate).*

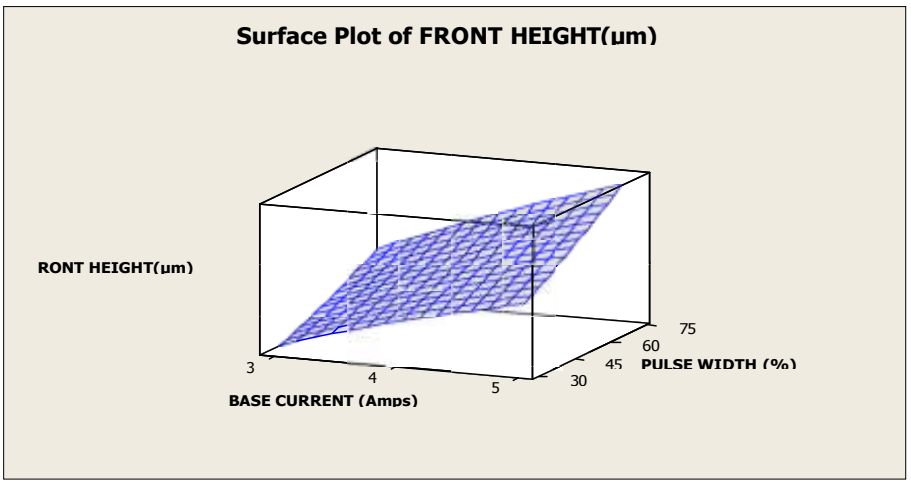

Fig. 13(e): *Surface plot for Front Height (Base Current versus Pulse Width).*

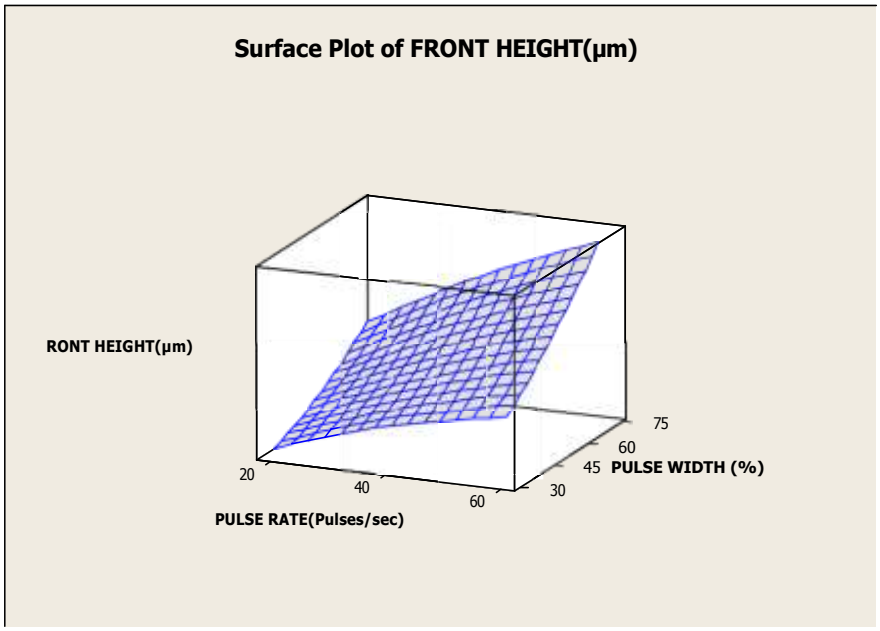

Fig. 13(f): *Surface plot for Front Height (Pulse Rate versus Pulse Width).*

Figures 14(a) to (f) represent the surface plots for back height.

From Figure 14(a), it is understood that back height is minimum at a peak current of 6 Amps and base current of 5 Amps.

From Figure 14(b), it is understood that back height is minimum at a peak current of 6 Amps and pulse rate of 60 pulses/sec.

From Figure 14(c), it is understood that back height is minimum at a peak current of 6 Amps and pulse width of 75%.

From Figure 14(d), it is understood that back height is maximum at a base current of 3 Amps and pulse rate of 60 pulses/sec.

From Figure 14(e), it is understood that back height is minimum at a base current of 3 Amps and pulse width of 60%.

From Figure 14(f), it is understood that back height is minimum at a pulse rate of 20 pulses/sec and pulse width of 70%.

From all the surface plots, it is understood that back height is minimum when peak current is 6 Amps, base current is 3 Amps, pulse rate of 60 pulses/sec and pulse width of 70%

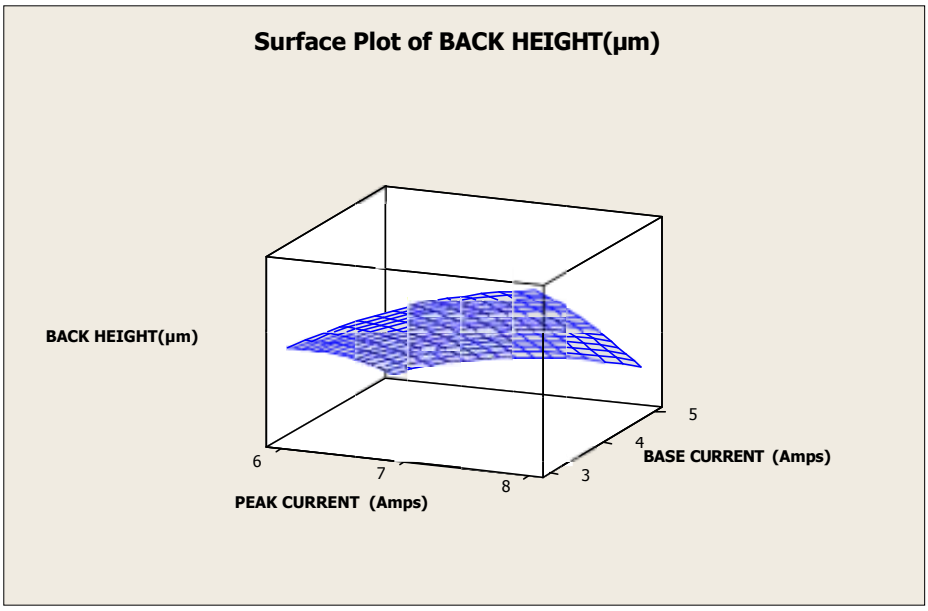

Fig. 14(a): *Surface plot for Back Height (Peak current versus Base Current).*

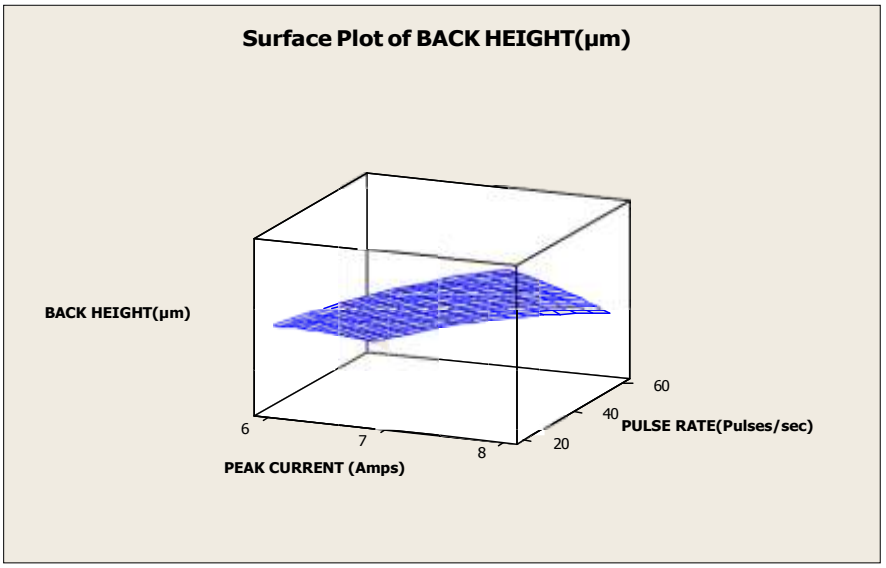

Fig. 14(b): *Surface plot for Back Height (Peak current versus Pulse Rate).*

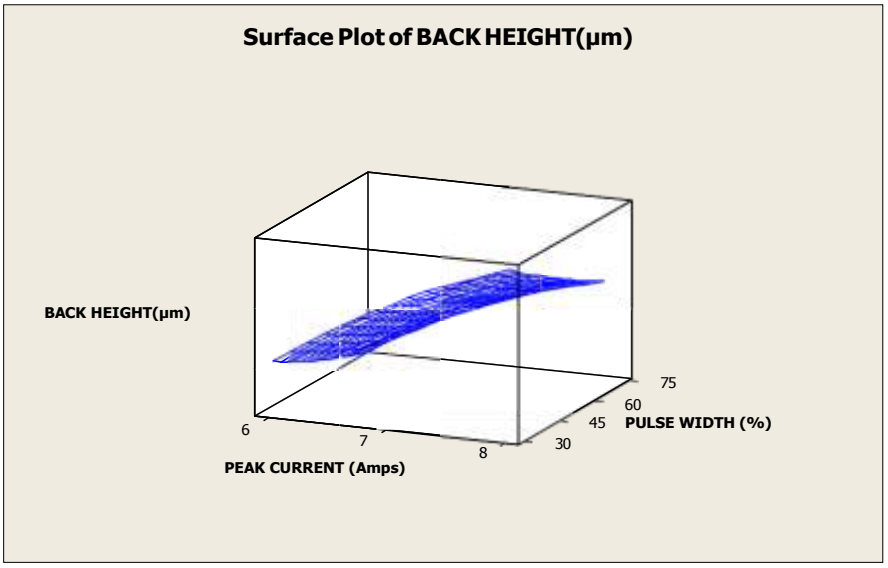

Fig. 14(c): *Surface plot for Back Height (Peak Current versus Pulse Width).*

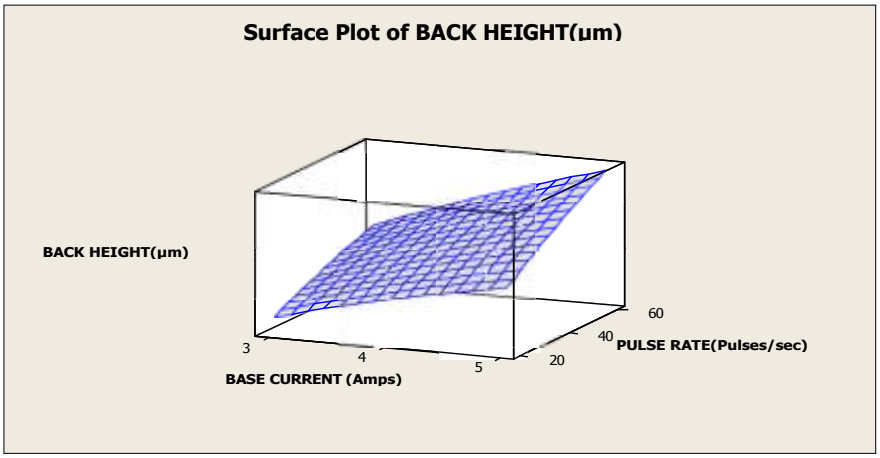

Fig. 14(d): *Surface plot for Back Height (Base Current versus Pulse Rate).*

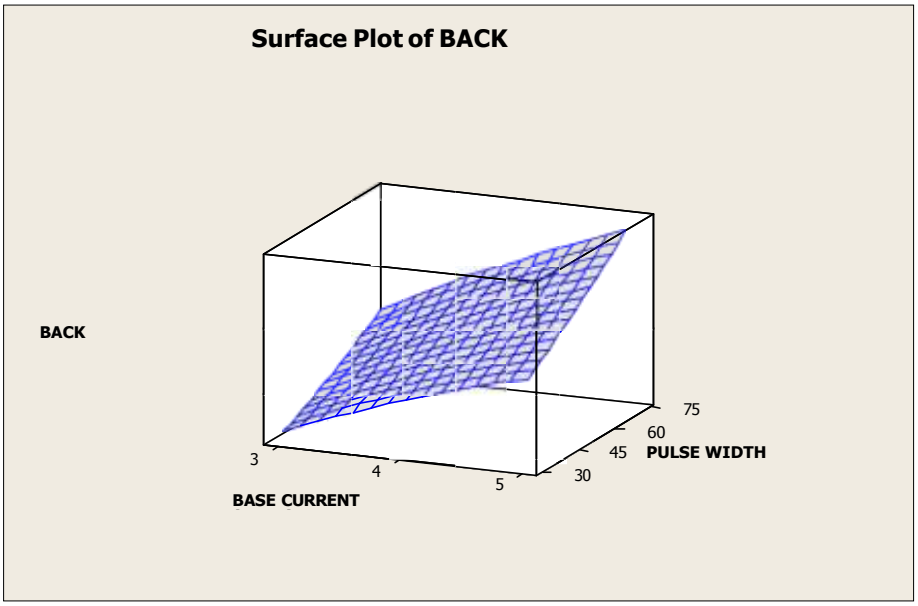

Fig. 14(e): *Surface plot for Back Height (Base Current versus Pulse Width)*

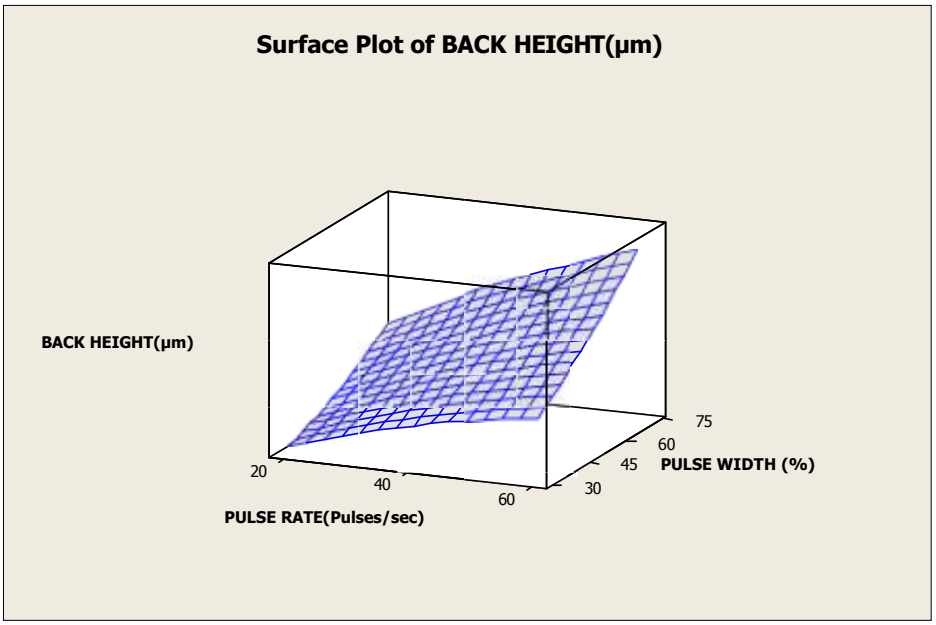

Fig. 14(f): *Surface plot for Back Height (Pulse Rate versus Pulse Width).*

CONCLUSIONS

From the experiments and developed models the following conclusions are drawn:

- Empirical mathematical models are developed for front width, back width, front height and back height of weld bead in order to predict their values within the range of the welding parameters selected for the chosen material (AISI 316Ti).
- The adequacy of the developed model is checked using ANOVA at 95% confidence level and found to be adequate.
- From the scatter plot it is understood that

experimental and predicted values are close to each other.

- Front width and back width increase with increase in peak current, back current and pulse rate. However they decrease with increase in pulse width.
- Front height and back height decrease with increase in peak current, back current and pulse rate. However they increase with increase in pulse width.
- From the surface plots of front width and back width, it is understood that maximum front width and back width can be achieved when peak current is 6 Amps, base current 3 Amps, pulse rate of 60 pulses/sec and pulse width of 70%.
- From the surface plots of front height and back height, it is understood that front height is minimum when peak current is 6 Amps, base current is 3 Amps, pulse rate of 60 pulses/sec and pulse width of 70%.
- From all the surface plots, it is understood that optimal weld bead geometry is obtained when peak current is 6 Amps, base current is 3 Amps, pulse rate of 60 pulses/sec and pulse width of 70%
- The developed mathematical models for weld bead geometry parameters are valid only for 0.3 mm thick AISI 316Ti austenitic stainless steel.
- The developed model is valid within the specified range of the selected welding parameters; however the accuracy can be improved by considering more number of factors and their levels.

REFERENCES

[1] Jean Marie Fortain. *Plasma Welding Evolution & Challenges.* Air Liquid CTAS, Welding and Cutting Research Center, 95315, Cergy Pontoise, France. 2010; 11p.

[2] Voropai NM, Shcherbak VV, Grigorev AA. Pulsed Microplasma Welding of Thin Aluminum Gaskets. *Equipment Manufacturing Technology*. 1971; 11: 19p.

[3] Sepokurov AS, Sergatskii GI, Alikin AP. Use of Microplasma Welding in Component Construction. *Japan Welding Society*. 1971; 11: 20p.

[4] Luo W. Effect of Micro-Plasma Arc Melting on the Corrosion Resistance of a 0Cr19Ni9 Stainless Steel SAW Joint. *Mater Lett*. 2002; 55: 290–295p.

[5] Karimzadeh F, Salehi M, Saatchi A, *et al.* Effect of Microplasma Arc Welding Process Parameters on Grain Growth and Porosity Distribution of Thin Sheet Ti6Al4V Alloy Weldment. *Mater Manuf Processes*. 2005; 20(2): 205–219p.

[6] Karimzadeh F, Ebnonnasir A, Foroughi A. Artificial Neural Network Modeling for Evaluating of Epitaxial Growth of Ti6Al4V Weldment. *Mater Sci Eng*. 2006; A 432: 184–190p.

[7] Pei-quan Xu, Shun Yao, Jian-Ping He, *et al.* Numerical Analysis for Effect of Process Parameters of Low-Current Micro-PAW on Constricted Arc. *Int J Adv Manuf Technol*. 2009; 44: 255–264p.

[8] Kondapalli Siva Prasad, Ch. Srinivasa Rao, Nageswara Rao D. Application of Grey Relational Analysis for Optimizing Weld Pool Geometry Parameters of Pulsed Current Micro Plasma Arc Welded Inconel 625 Sheets. *Int J Adv Manuf Technol*, (Springer). 2015. DOI: 10.1007/s00170-014-6665-y.

[9] Siva Prasad K, Ch. Srinivasa Rao, Nageswara Rao D. Effect of Process Parameters of Pulsed Current Micro Plasma Arc Welding on Weld Pool Geometry of Inconel 625 Welds. *Kovove Materialy-Metallic Materials (Kovove Mater).* 2012; 0(3): 153–159p.

[10] Kondapalli Siva Prasad, Ch. Srinivasa Rao, Nageswara Rao D. Application of Grey Relational Analysis for Optimizing Weld Pool Geometry Parameters of Pulsed Current Micro Plasma Arc Welded AISI 304L Stainless Steel Sheets. *Int J Adv Des Manuf Technol*. 2013; 6(1): 79–86p.